Unified Approach to Wave Diffraction by Space–Time Periodic Anisotropic Media

KATSU ROKUSHIMA, MEMBER, IEEE, JIRO YAMAKITA, SHIZUO MORI, AND KENJI TOMINAGA

Abstract—**The diffraction properties of electromagnetic waves propagating in a planar anisotropic medium with tensor permittivity which is modulated periodically with respect to space and time are analyzed by extending the previous theory for time-invariant anisotropic dielectric gratings. The method applies to any isotropic or anisotropic medium, any polarization of the incident plane wave, and any orientation of the grating vector. The analysis is formulated in a unified matrix form so that calculations can be performed systematically. As numerical examples of the general analysis, the optical diffractions by an acoustic wave in a birefringent crystal and by a cholesteric liquid crystal are treated, where the approximate two-wave analysis is also derived and the accuracy is discussed by comparison with the rigorous analysis.**

I. Introduction

OPTICAL DIFFRACTION by planar dielectric gratings has been extensively studied for many years. Analysis for these periodic structures plays an important role as the basis of integrated optics, acousto-optics, holography, and liquid crystal structures. There have been numerous papers on the subject of grating diffraction with many different analytic methods [1]–[7]; these are summarized in the references of the [7]. However, to the authors' knowledge, most of the rigorous analysis has been limited to the case of isotropic gratings, with only slight attention given to gratings.

Dixon [8] has considered anisotropic Bragg diffraction by traveling acoustic waves in optically anisotropic crystals and has given an approximate solution for diffracted intensity. Hope [9] has also discussed Brillouin scattering by acoustic waves in birefringent media using integral equation methods. However the results are given in somewhat complicated form and the numerical calculations are based on an approximate two-wave analysis. The wave propagation and dispersion in several periodic liquid crystal structures have also been studied extensively and the results are given by the rigorous numerical 4×4 matrix method [10], by approximate dynamic theory [11], [12], and by exact and approximate analytic methods [13]–[15]. The 4×4 matrix method has also been applied to wave propagation in birefringent layered media [16]. However, those analyses are limited to the case where the grating vector is perpendicular to the slab surface.

The authors have proposed a rigorous analysis for spatially periodic anisotropic media [17]. In this paper the previous method is extended to cover both space- and time-periodic anisotropic media, and the analysis is formulated in a unified matrix form. As applications of the general theory, the numerical results are given for optical diffraction by an acoustic wave in a birefringent crystal and by a cholesteric liquid crystal. The approximate two-wave analysis for a special case is also derived and the accuracy of the numerical calculations is discussed.

Manuscript received March 20, 1986; revised July 17, 1987.

K. Rokushima, J. Yamakita, and S. Mori are with the Department of Electrical Engineering, College of Engineering, University of Osaka Prefecture, Sakai, Osaka, Japan.

K. Tominaga was with the Department of Electrical Engineering, University of Osaka Prefecture. He is now with the Mitsubishi Electric Co., Ltd., Tokyo, Japan.

IEEE Log Number 8716919.

II. Analysis

As shown in Fig. 1, we consider the optical diffraction by a space-time periodic anisotropic medium bounded by two isotropic uniform media with relative permittivity ϵ_I $(I=1,3)$. For the incidence of a generally polarized wave in the xz plane with an angle of incidence θ_i, all the field components of the incident wave have the form of $\exp[j\{\omega_0 t - \sqrt{\epsilon_1}\, k_0(x\cos\theta_i + z\sin\theta_i)\}]$, where ω_0 is the optical angular frequency and $k_0 = \omega_0\sqrt{\epsilon_0\mu_0} = 2\pi/\lambda$ is the wavenumber in vacuum.

A. Electromagnetic Fields in the Space–Time Periodic Anisotropic Medium

The relative tensor permittivity $\hat{\epsilon}$ of the medium with permeability μ_0 is given by

$$\hat{\epsilon} = [\epsilon_{ij}] = \begin{bmatrix} \epsilon_{xx} & \epsilon_{xy} & \epsilon_{xz} \\ \epsilon_{yx} & \epsilon_{yy} & \epsilon_{yz} \\ \epsilon_{zx} & \epsilon_{zy} & \epsilon_{zz} \end{bmatrix} \tag{1}$$

with

$$\epsilon_{ij}(\boldsymbol{r}, t) = \sum_l \epsilon_{ij,l} \exp\{jl(\boldsymbol{K}\cdot\boldsymbol{r} - \Omega t)\} \qquad (i, j = x, y, z) \tag{2}$$

where $\boldsymbol{K}$ is the grating vector having any orientation in three dimensions, $|\boldsymbol{K}| = K = 2\pi/\Lambda$, Λ is the space period, Ω is the angular frequency, and $\epsilon_{ij,l}$ is the lth order Fourier coefficients known for a given medium. Thus, in a crystal traversed by a traveling acoustic wave with a constant phase velocity $v = \Omega/K$, the relative permittivity is given by $\hat{\epsilon}(\boldsymbol{r}\cdot t)$. A similar space-periodic variation of $\hat{\epsilon}(\boldsymbol{r})$ with $\Omega = 0$ exists in a liquid crystal structure. As in the previous paper, we normalize the space and time variables

0018-9480/87/1100-0937$01.00

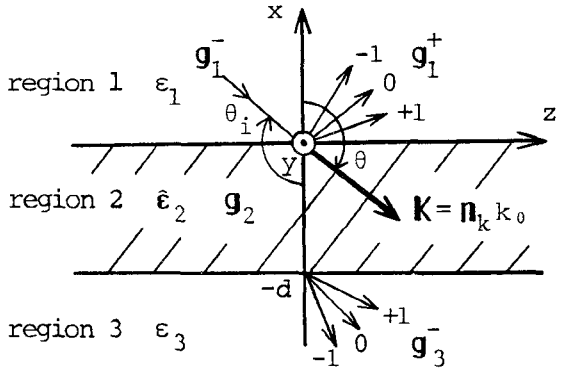

Fig. 1. Geometry of wave diffraction by a space-time periodic medium.

by k_0 and ω_0, respectively, putting $k_0 \boldsymbol{r} \to \boldsymbol{r}(k_0 x \to x, k_0 y \to y, k_0 z \to z)$ and $\omega_0 t \to t$. For simplicity, these normalized variables are used unless otherwise stated. Then, Maxwell's equations are expressed as

$$\begin{aligned} \operatorname{curl} \sqrt{Y_0}\boldsymbol{E} &= -\partial\left(\sqrt{Z_0}\boldsymbol{H}\right)/\partial t \\ \operatorname{curl} \sqrt{Z_0}\boldsymbol{H} &= \partial\left(\hat{\boldsymbol{\epsilon}}(\boldsymbol{r}\cdot t)\sqrt{Y_0}\boldsymbol{E}\right)/\partial t \end{aligned} \tag{3}$$

where $Y_0 = 1/Z_0 = \sqrt{\epsilon_0/\mu_0}$ and

$$\epsilon_{ij}(\boldsymbol{r}, t) = \sum_l \epsilon_{ij,l} \exp\{jl(\boldsymbol{n}_k \cdot \boldsymbol{r} - \omega_r t)\} \tag{4}$$

with

$$\begin{aligned} \boldsymbol{n}_k &= \boldsymbol{K}/k_0 = \boldsymbol{i}_x p + \boldsymbol{i}_y q + \boldsymbol{i}_z s \\ |\boldsymbol{n}_k| &= n_k = \lambda/\Lambda \\ \omega_r &= \Omega/\omega_0. \end{aligned} \tag{5}$$

Here $\boldsymbol{i}_i$ $(i = x, y, z)$ is the unit vector along the i axis.

Taking into account the phase matching condition at the interfaces for the incidence of a plane wave, electric and magnetic fields can be expanded by the space-time harmonics from the Floquet theorem:

$$\begin{aligned} \sqrt{Y_0}\boldsymbol{E} &= \sum_m \boldsymbol{e}_m(x) \exp\{-j(\boldsymbol{n}_m \cdot \boldsymbol{r} - \omega_m t)\} \\ \sqrt{Z_0}\boldsymbol{H} &= \sum_m \boldsymbol{h}_m(x) \exp\{-j(\boldsymbol{n}_m \cdot \boldsymbol{r} - \omega_m t)\} \end{aligned} \tag{6}$$

where the index m under the summation sign is understood to run over all values of $m = 0, \pm 1, \pm 2, \cdots$ and

$$\boldsymbol{e}_m(x) = \sum_i \boldsymbol{i}_i e_{im}(x) \qquad \boldsymbol{h}_m(x) = \sum_i \boldsymbol{i}_i h_{im}(x) \tag{7}$$

$$\begin{aligned} \boldsymbol{n}_m &= \boldsymbol{i}_x p_m + \boldsymbol{i}_y q_m + \boldsymbol{i}_z s_m \\ p_m &= p_0 + mp \qquad q_m = mq \qquad s_m = s_0 + ms \\ s_0 &= \sqrt{\epsilon_1}\sin\theta_i \end{aligned} \tag{8}$$

$$\omega_m = 1 + m\omega_r. \tag{9}$$

Here p_0 is arbitrary and can be set equal to zero.

By substituting (6) into (3), multiplying $\exp\{j(\boldsymbol{n}_m \cdot \boldsymbol{r} - \omega_m t)\}$ on both sides and integrating over y, z, and t for each period, we get the following coupled-wave equations in matrix form (Appendix I), as in the time-invariant gratings [17]:

$$\frac{d}{dx}\boldsymbol{f}_t = j\boldsymbol{C}\boldsymbol{f}_t \qquad \boldsymbol{f}^n = \boldsymbol{D}\boldsymbol{f}_t \tag{10}$$

$$\boldsymbol{f}_t = \begin{bmatrix} \boldsymbol{e}_y \\ \boldsymbol{h}_z \\ \boldsymbol{e}_z \\ \boldsymbol{h}_y \end{bmatrix} \qquad \boldsymbol{f}_n = \begin{bmatrix} \boldsymbol{e}_x \\ \boldsymbol{h}_x \end{bmatrix}. \tag{11}$$

Here $\boldsymbol{f}_t$ and $\boldsymbol{f}_n$ are column matrices consisting of the space-time harmonics of the tangential and normal field components to the slab surface, and $\boldsymbol{e}_i = \boldsymbol{e}_i(x)$ and $\boldsymbol{h}_i = \boldsymbol{h}_i(x)$ are column matrices with elements $e_{im}(x)$ and $h_{im}(x)$. $\boldsymbol{C}$ and $\boldsymbol{D}$ are coupling matrices expressing the interaction of the space-time harmonics and are given by

$$\boldsymbol{C} = \begin{bmatrix} \boldsymbol{C}_{11} & \boldsymbol{C}_{12} \\ \boldsymbol{C}_{21} & \boldsymbol{C}_{22} \end{bmatrix} \tag{12}$$

with

$$\begin{aligned} \boldsymbol{C}_{11} &= \begin{bmatrix} \boldsymbol{q}\boldsymbol{\epsilon}_{xx}^{-1}\boldsymbol{\epsilon}_{xy} + \boldsymbol{p} & \boldsymbol{q}\boldsymbol{\epsilon}_{xx}^{-1}\boldsymbol{q}\boldsymbol{\omega}^{-1} - \boldsymbol{\omega} \\ \boldsymbol{\omega}\left(\boldsymbol{\epsilon}_{vx}\boldsymbol{\epsilon}_{xx}^{-1}\boldsymbol{\epsilon}_{xy} - \boldsymbol{\epsilon}_{yy}\right) + \boldsymbol{s}^2\boldsymbol{\omega}^{-1} & \boldsymbol{\omega}\boldsymbol{\epsilon}_{yx}\boldsymbol{\epsilon}_{xx}^{-1}\boldsymbol{q}\boldsymbol{\omega}^{-1} + \boldsymbol{p} \end{bmatrix} \\ \boldsymbol{C}_{21} &= \begin{bmatrix} \boldsymbol{s}\boldsymbol{\epsilon}_{xx}^{-1}\boldsymbol{\epsilon}_{xy} & \boldsymbol{s}\boldsymbol{\epsilon}_{xx}^{-1}\boldsymbol{q}\boldsymbol{\omega}^{-1} \\ \boldsymbol{\omega}\left(\boldsymbol{\epsilon}_{zy} - \boldsymbol{\epsilon}_{zx}\boldsymbol{\epsilon}_{xx}^{-1}\boldsymbol{\epsilon}_{xy}\right) + \boldsymbol{q}\boldsymbol{s}\boldsymbol{\omega}^{-1} & -\boldsymbol{\omega}\boldsymbol{\epsilon}_{zx}\boldsymbol{\epsilon}_{xx}^{-1}\boldsymbol{q}\boldsymbol{\omega}^{-1} \end{bmatrix} \\ \boldsymbol{C}_{12} &= \begin{bmatrix} \boldsymbol{q}\boldsymbol{\epsilon}_{xx}^{-1}\boldsymbol{\epsilon}_{xz} & -\boldsymbol{q}\boldsymbol{\epsilon}_{xx}^{-1}\boldsymbol{\omega}^{-1}\boldsymbol{s} \\ \boldsymbol{\omega}\left(\boldsymbol{\epsilon}_{yx}\boldsymbol{\epsilon}_{xx}^{-1}\boldsymbol{\epsilon}_{xz} - \boldsymbol{\epsilon}_{yz}\right) - \boldsymbol{s}\boldsymbol{q}\boldsymbol{\omega}^{-1} & -\boldsymbol{\omega}\boldsymbol{\epsilon}_{yx}\boldsymbol{\epsilon}_{xx}^{-1}\boldsymbol{s}\boldsymbol{\omega}^{-1} \end{bmatrix} \\ \boldsymbol{C}_{22} &= \begin{bmatrix} \boldsymbol{s}\boldsymbol{\epsilon}_{xx}^{-1}\boldsymbol{\epsilon}_{xz} + \boldsymbol{p} & \boldsymbol{\omega} - \boldsymbol{s}\boldsymbol{\epsilon}_{xx}^{-1}\boldsymbol{s}\boldsymbol{\omega}^{-1} \\ \boldsymbol{\omega}\left(\boldsymbol{\epsilon}_{zz} - \boldsymbol{\epsilon}_{zx}\boldsymbol{\epsilon}_{xx}^{-1}\boldsymbol{\epsilon}_{xz}\right) - \boldsymbol{q}^2\boldsymbol{\omega}^{-1} & \boldsymbol{\omega}\boldsymbol{\epsilon}_{zx}\boldsymbol{\epsilon}_{xx}^{-1}\boldsymbol{s}\boldsymbol{\omega}^{-1} + \boldsymbol{p} \end{bmatrix} \end{aligned} \tag{13}$$

$$\boldsymbol{D} = \begin{bmatrix} -\boldsymbol{\epsilon}_{xx}^{-1}\boldsymbol{\epsilon}_{xy} & -\boldsymbol{\epsilon}_{xx}^{-1}\boldsymbol{q}\boldsymbol{\omega}^{-1} & -\boldsymbol{\epsilon}_{xx}^{-1}\boldsymbol{\epsilon}_{xz} & \boldsymbol{\epsilon}_{xx}^{-1}\boldsymbol{s}\boldsymbol{\omega}^{-1} \\ -\boldsymbol{s}\boldsymbol{\omega}^{-1} & \boldsymbol{0} & \boldsymbol{q}\boldsymbol{\omega}^{-1} & \boldsymbol{0} \end{bmatrix} \tag{14}$$

where

$$\begin{aligned} \boldsymbol{\epsilon}_{ij} &= [\epsilon_{ij,lm}] = [\epsilon_{ij,m-l}] \\ \boldsymbol{p} &= [\delta_{lm}p_m] \qquad \boldsymbol{q} = [\delta_{lm}q_m] \qquad \boldsymbol{s} = [\delta_{lm}s_m] \\ \boldsymbol{\omega} &= [\delta_{lm}\omega_m] \qquad \boldsymbol{1} = [\delta_{lm}]. \end{aligned} \tag{15}$$

Here, $\boldsymbol{C}$ is a $4(2m+1)\times 4(2m+1)$ matrix, $\boldsymbol{D}$ is a $4(2m+1)\times 2(2m+1)$ matrix, and $\boldsymbol{C}_{mn}$ are $2(2m+1)\times 2(2m+1)$ matrices, while $\boldsymbol{\epsilon}_{ij}$ are $(2m+1)\times(2m+1)$ submatrices, $\boldsymbol{\epsilon}_{ij}^{-1}$ are the inverse matrices of $\boldsymbol{\epsilon}_{ij}$ and, $\boldsymbol{p}$, $\boldsymbol{q}$, $\boldsymbol{s}$, $\boldsymbol{\omega}$, and $\boldsymbol{1}$ are $(2m+1)\times(2m+1)$ diagonal submatrices, where δ_{lm} is the Kronecker delta. For isotropic gratings $\boldsymbol{\epsilon}_{ij} = \delta_{ij}\boldsymbol{\epsilon}$. The appearance of $\boldsymbol{\omega}$ in the coupling matrices $\boldsymbol{C}$ and $\boldsymbol{D}$ is due to the Doppler effect, by which the angular frequency of the mth-order diffracted wave is shifted to $\omega_0(1 + m\omega_r)$. For time-invariant gratings, $\boldsymbol{\omega} = \boldsymbol{1}$.

In the usual two-dimensional case in which the grating vector $\boldsymbol{K}$ lies in the plane of incidence (xz plane), $\boldsymbol{q} = \boldsymbol{0}$ and the plane of diffraction is also in the xz plane. Then, $\boldsymbol{C}_{11}$ expresses the coupling between TE waves (with $\boldsymbol{e}_y, \boldsymbol{h}_x, \boldsymbol{h}_z$ components) and $\boldsymbol{C}_{22}$ expresses the coupling

between TM waves (with e_x, e_z, h_y components), while C_{12} and C_{21} express the mutual coupling between TE and TM waves. Moreover, when ϵ_{ij} $(i \neq j) = 0$, $C_{12} = C_{21} = 0$ and then the problem can be solved separately for TE or TM waves by using only C_{11} or C_{22}.

By transforming

$$f_t = Tg \tag{16}$$

(10) is reduced to

$$\frac{d}{dx} g = j\kappa g. \tag{17}$$

Here, $\kappa = [\delta_{mn}\kappa_n]$ is a diagonal matrix, with $\kappa_n = \kappa_{n'}^{\pm}$, the eigenvalues of the $n \times n$ matrix C, where $n = 2n' = 4(2m+1)$. $T = [T^+ T^-] = [U_1^+ \cdots U_{n'}^+ U_1^- \cdots U_{n'}^-]$ is the diagonalizer of C with eigenvectors $U_{n'}^{\pm}$ corresponding to $\kappa_{n'}^{\pm}$, and g is a column matrix with elements $g_{n'}^{\pm}$. Equation (10) has eigensolutions $U_{n'}^{\pm} \exp(j\kappa_{n'}^{\pm} x) g_{n'}^{\pm}$ which correspond to the optical eigenmodes traveling along the $\pm x$ directions.

B. Electromagnetic Fields in the Uniform Isotropic Medium

In the uniform isotropic region, $\epsilon_{ij} = \delta_{ij}\epsilon \mathbf{1}$ and $p = 0$ in (13), and then C becomes C^u with all the diagonal submatrices. The diagonalizer T^u for C^u is explicitly given by

$$T^u = \begin{bmatrix} \dot{s} & (1/\sqrt{\epsilon})\xi\dot{q} & \dot{s} & (1/\sqrt{\epsilon})\xi\dot{q} \\ \dot{s}\xi & \sqrt{\epsilon}\,\dot{q} & -\dot{s}\xi & -\sqrt{\epsilon}\,\dot{q} \\ -\dot{q} & (1/\sqrt{\epsilon})\xi\dot{s} & -\dot{q} & (1/\sqrt{\epsilon})\xi\dot{s} \\ \dot{q}\xi & -\sqrt{\epsilon}\,\dot{s} & -\dot{q}\xi & \sqrt{\epsilon}\,\dot{s} \end{bmatrix} = [T^{u+} \quad T^{u-}] \tag{18}$$

with diagonal submatrices $\dot{q} = [\delta_{lm}\dot{q}_m]$, $\dot{s} = [\delta_{lm}\dot{s}_m]$, and $\xi = [\delta_{lm}\xi_m/\omega_m]$, where $\kappa_m^{u\pm} = \mp\xi_m = \mp\sqrt{\omega_m^2\epsilon - n_{tm}^2}$ is the eigenvalue of C^u, $n_{tm} = \sqrt{s_m^2 + p_m^2}$, $\dot{q}_m = q_m/n_{tm}$, $\dot{s}_m = s_m/n_{tm}$, and the corresponding g is expressed as

$$g = \begin{bmatrix} g^+ \\ g^- \end{bmatrix} = \begin{bmatrix} {}^{\mathrm{E}}g^+ \\ {}^{\mathrm{M}}g^+ \\ {}^{\mathrm{E}}g^- \\ {}^{\mathrm{M}}g^- \end{bmatrix} \tag{19}$$

$$ {}^{\mathrm{E}}g^{\pm} = [{}^{\mathrm{E}}g_{-m}^{\pm} \cdots {}^{\mathrm{E}}g_0^{\pm} \cdots {}^{\mathrm{E}}g_m^{\pm}]^t$$
$$ {}^{\mathrm{M}}g^{\pm} = [{}^{\mathrm{M}}g_{-m}^{\pm} \cdots {}^{\mathrm{M}}g_0^{\pm} \cdots {}^{\mathrm{M}}g_m^{\pm}]^t. \tag{20}$$

Here, the field amplitudes of each eigenmode in the uniform region are normalized to $|{}^{\mathrm{E}}e_m| = |{}^{\mathrm{M}}e_m| = 1$. The superscripts E and M refer to TE and TM waves, and the signs $\pm$ refer to the propagation along the $\pm x$ directions.

The mth-order eigenmode expresses a TE or a TM plane wave of the form $\exp[-j(\pm\xi_m x + q_m y + s_m z)]$ whose frequency is shifted to ω_m. In the two-dimensional case, TE waves have tangential field components of e_y and h_z while TM waves have those of e_z and h_y. However, in the three-dimensional case, both TE and TM waves have all field components because the plane of diffraction does not lie in the xz plane [17].

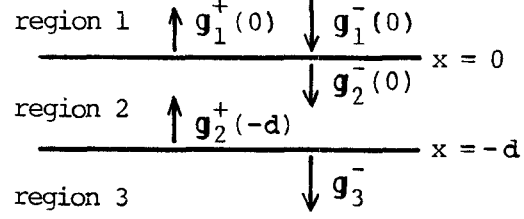

Fig. 2. Boundary surfaces and unknowns.

C. Boundary Conditions

Within regions I $(I = 1,2,3)$, the solution of (17) is given by

$$\begin{bmatrix} g_I^+(x) \\ g_I^-(x) \end{bmatrix} = \begin{bmatrix} \exp[j\kappa_I^+(x - x_0)] & 0 \\ 0 & \exp[j\kappa_I^-(x - x_0)] \end{bmatrix} \cdot \begin{bmatrix} g_I^+(x_0) \\ g_I^-(x_0) \end{bmatrix} \tag{21}$$

where $\exp[j\kappa_I^{\pm}(x - x_0)] = [\delta_{mn'}\exp\{j\kappa_{In'}^{\pm}(x - x_0)\}]$ are diagonal matrices and $g_I^{\pm}(x_0)$ are constant column matrices at $x = x_0$.

At the boundary surfaces ($x = 0$ and $x = -d$), tangential components of the fields $\sqrt{Y_0}E$ and $\sqrt{Z_0}H$ are continuous; that is, $f_{t1}(0) = f_{t2}(0)$ and $\exp(jp_2 d) f_{t2}(-d) = f_{t3}(-d)$, where $\exp[jp_2 d]$ is a diagonal matrix with four diagonal submatrices $\exp[jp_2 d] = [\delta_{1m}\exp(jp_{2m}d)]$. Since $\kappa_{n'}^{\pm}$ have complex values $(\mathrm{Im}\{\kappa_{n'}^{\pm}\} \gtrless 0)$, $\exp(\mp j\kappa_{n'}^{\pm}, d)$ may become very large for higher order $\kappa_{n'}^{\pm}$. Therefore, boundary conditions have been expressed in somewhat modified form in order to avoid overflow problems in the numerical computation. Thus, from (6), (11), and (21), and taking $g_2^-(0)$ and $g_2^+(-d)$ as the unknowns in region 2 as in Fig. 2, we get

$$\begin{bmatrix} -T_1^{u+} & B_{12}^+ & 0 \\ 0 & B_{23}^- & T_3^{u-} \end{bmatrix} \begin{bmatrix} g_1^+(0) \\ g_2^+(-d) \\ g_2^-(0) \\ g_3^-(-d) \end{bmatrix} = \begin{bmatrix} T_1^{u-} g_1^-(0) \\ 0 \end{bmatrix} \tag{22}$$

with

$$B_{12}^+ = T_2 \begin{bmatrix} \exp[j\kappa_2^+ d] & 0 \\ 0 & 1 \end{bmatrix}$$
$$B_{23}^- = -\exp[jp_2 d] T_2 \begin{bmatrix} 1 & 0 \\ 0 & \exp[-j\kappa_2^- d] \end{bmatrix}. \tag{23}$$

D. Diffraction Efficiency

From (22), diffracted waves $g_1^+(0)$ and $g_3^-(-d)$ are obtained for the incidence of a TE or TM wave:

$${}^{\mathrm{E,M}}g_1^-(0) = [0 \cdots 1 \cdots 0]^t \qquad {}^{\mathrm{M,E}}g_1^-(0) = 0. \tag{24}$$

The mth-order powers along the $\pm x$ directions in regions

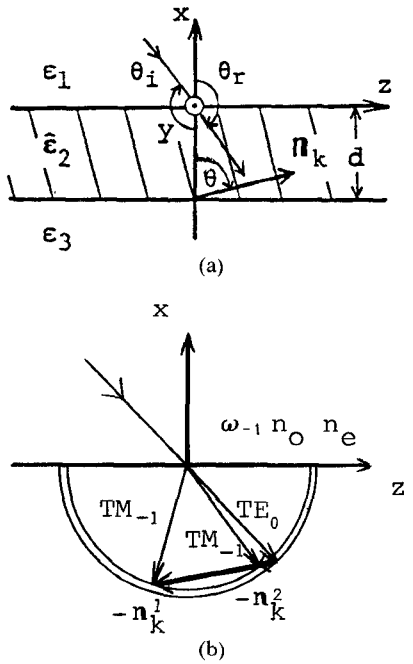

Fig. 3. Optical diffraction by an acoustic wave in a crystal. (a) Geometry. (b) Forward Bragg diffraction.

I ($I=1,3$) are given by, for both TE and TM waves,

$$^{E,M}P_{Im}^{\pm} = \mathrm{Re}(\xi_{Im})|^{E,M}g_{Im}^{\pm}|^2/\omega_m. \tag{25}$$

Therefore, the mth-order diffraction efficiencies of the transmitted and reflected waves $\eta_m^{t,r} = P_{Im}^{\pm}/P_{10}$ are given for arbitrary orientation of the waves.

For a lossless and time-invariant medium, the power conservation relation requires $\Sigma_m \Sigma_{E,M}(\eta_m^r + \eta_m^t) = 1$, which can be used as a check for the numerical calculations. However, for a time-periodic medium pumped by external source (for instance, by an acoustic wave), this relation does not hold because energy transfer occurs due to the parametric coupling in the medium.

III. Numerical Results

A. Optical Diffraction by an Acoustic Wave

As shown in Fig. 3, we assume that an acoustic shear wave polarized along the y axis propagates in the xz plane with the propagation vector $\boldsymbol{K}$ inclined to the slab normal at an angle θ. The medium in the slab has a uniaxial wurtzite crystal structure with its optic axis along the y direction. Coordinates are chosen such that the x, y, and z axes are along the [010], [001], and [100] directions, respectively.

The acoustic wave is given by

$$\boldsymbol{u}(\boldsymbol{r},t) = \boldsymbol{i}_y A \sin(\boldsymbol{n}_k \cdot \boldsymbol{r} - \omega_r t) \tag{26}$$

where

$$\begin{aligned} \boldsymbol{K}/k_0 = \boldsymbol{n}_k &= \boldsymbol{i}_x p + \boldsymbol{i}_z s \\ &= n_k(\boldsymbol{i}_x \cos\theta + \boldsymbol{i}_z \sin\theta). \end{aligned} \tag{27}$$

The components of the strain tensor S_{ij} due to the acoustic wave is given by $S_{ij}\cos(\boldsymbol{n}_k \cdot \boldsymbol{r} - \omega_r t)$, where $S_{ij} = \frac{1}{2}(A_i K_j + A_j K_i)$. The strain induces a small periodic variation $\Delta\hat{\epsilon}(\boldsymbol{r},t)$ in the tensor permittivity $\hat{\epsilon}$. This effect is usually described in terms of photo-elastic coefficients p_{klmn} and is given by [9]

$$\begin{aligned} \Delta\epsilon_{ij}(\boldsymbol{r},t) &= \Delta\epsilon_{ij}\cos(\boldsymbol{n}_k \cdot \boldsymbol{r} - \omega_r t) \\ \Delta\epsilon_{ij} &= -\epsilon_{ik}\epsilon_{jl}p_{klmn}S_{mn} \end{aligned} \tag{28}$$

where ϵ_{ij} are the elements of tensor permittivity in the absence of strain. In this coordinate system, the acoustic wave with $A = A_y = A_3$, $K_x = K_2$, and $K_z = K_1$ produces components of the strain tensor $S_4 = AK_x$ and $S_5 = AK_z$, which produce nondiagonal elements ϵ_{xy} and ϵ_{yz} in the original permittivity tensor by (28), where customary abbreviations of indices 4 = (23) = (32), 5 = (13) = (31), $P_{44} = P_{2323}$ and the fact $P_{1313} = P_{2323}$ are used. Therefore elements of $\hat{\epsilon}$ in region 2 are given by

$$\begin{aligned} &\epsilon_{xx} = \epsilon_{zz} = n_o^2 \qquad \epsilon_{yy} = n_e^2 \\ &\epsilon_{xy} = \epsilon_{yx} = \delta n_o n_e \cos\theta \cos(\boldsymbol{n}_k \cdot \boldsymbol{r} - \omega_r t) \\ &\epsilon_{yz} = \epsilon_{zy} = \delta n_o n_e \sin\theta \cos(\boldsymbol{n}_k \cdot \boldsymbol{r} - \omega_r t) \end{aligned} \tag{29}$$

where n_o and n_e are ordinary and extraordinary refractive indices of the crystal without strain, respectively, and the change in the dielectric permittivity is put to $-n_o^2 n_e^2 P_{44} KA = \delta n_o n_e$. The elements ϵ_{ij} in $\boldsymbol{C}$ of (13) become, in matrix form, for instance,

$$\epsilon_{xx} = n_0^2 \begin{bmatrix} & & \vdots & & & \\ & 1 & 0 & 0 & 0 & \\ & 0 & 1 & 0 & 0 & \\ \cdots & & & & & \cdots \\ & 0 & 0 & 1 & 0 & \\ & 0 & 0 & 0 & 1 & \\ & & \vdots & & & \end{bmatrix},$$

$$\epsilon_{xy} = \frac{\delta}{2} n_o n_e \cos\theta \begin{bmatrix} & & & \vdots & & \\ & & 0 & 1 & 0 & 0 & \\ & & 1 & 0 & 1 & 0 & \\ \cdots & & & & & & \cdots \\ & & 0 & 1 & 0 & 1 & \\ & & 0 & 0 & 1 & 0 & \\ & & & \vdots & & & \end{bmatrix}, \text{ etc.} \tag{30}$$

Due to ϵ_{xy} and ϵ_{yz}, TE–TM mode conversion takes place in this forward diffraction. For the incidence of an TE wave, the Mth-order Bragg condition between TE and TM waves is given by [18], [19]

$$\begin{aligned} Mn_k^{1,2} &= -n_e\cos(\theta_r - \theta) \pm \sqrt{n_e^2\cos^2(\theta_r - \theta) + \omega_M^2 n_o^2 - n_e^2} \\ \omega_M &= 1 + M\omega_r \end{aligned} \tag{31}$$

where θ_r is the refraction angle given by $\sqrt{\epsilon_1}\sin\theta_i = n_e \sin\theta_r$.

The diffraction efficiencies of the transmitted waves η_m^t for the incidence of a TE wave at the first-order Bragg condition ($M=-1$) are shown in Figs. 4–6. Calculations were performed by using the parameter values of $n_e = 2.470$, $n_o = 2.453$ (CdS), $n_k^1 = 0.74557$, $n_k^2 = 0.11225$, $\delta = 0.1$, $\theta = 80°$, and $\theta_i = 160°$, and by putting $\omega = \mathbf{1}$ ($\Omega \ll \omega_0$). The parameter values of the uniform regions are chosen as $\epsilon_1 = \epsilon_3 = n_e^2$ to minimize the effect of the boundary reflec-

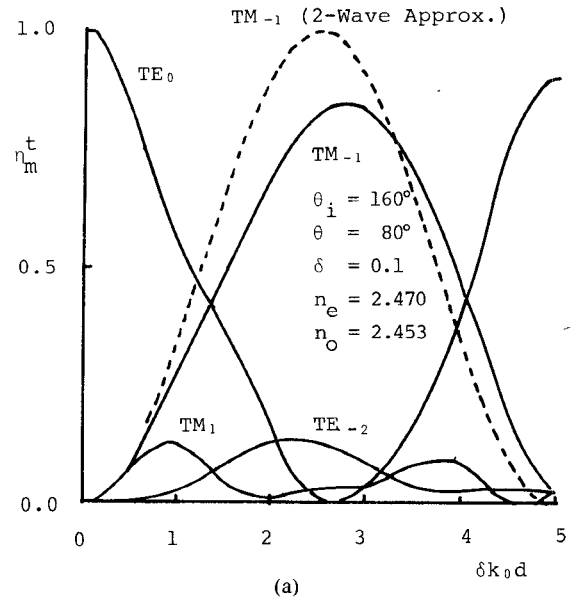

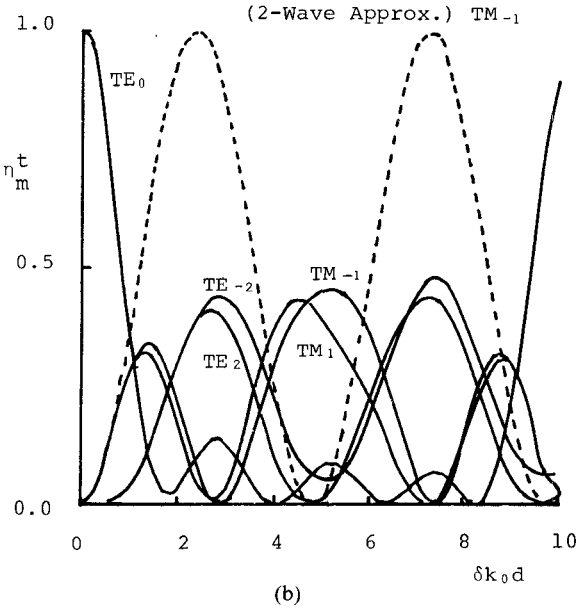

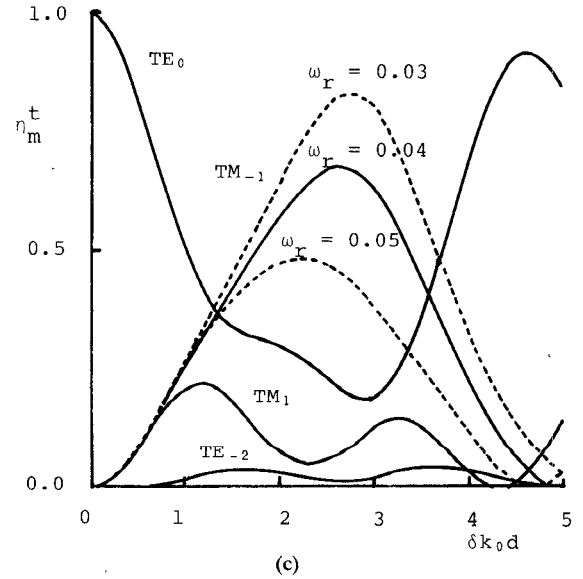

Fig. 4. The diffraction efficiencies of transmitted waves for the incidence of a TE wave at the first-order Bragg condition. (a) $n_k^1 = 0.74557$, (b) $n_k^2 = 0.11225$, and (c) $n_k^1 = 0.74557$ with $\omega_r = 0.03 \sim 0.05$.

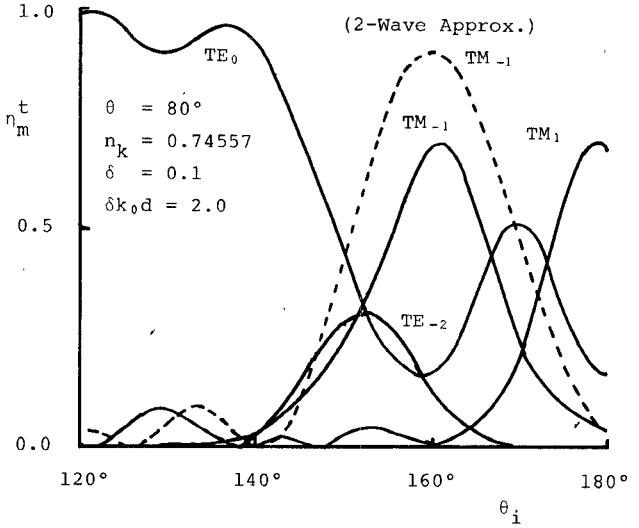

Fig. 5. Variation of the diffraction efficiencies with the angle of incidence.

tion and to compare with the approximate two-wave analysis.

Figs. 4 and 5 show the variation of η_m^t with the index normalized thickness of the grating $\delta k_0 d$ and with the angle of incidence θ_i. The calculations were performed by retaining up to $\bar{m} = 3$, where $\bar{m}$ is the order of harmonics taken into the calculations, that is, $m = 0, \pm 1, \cdots, \pm \bar{m}$. The error in the power-conservation relation was of the order of 10^{-8} in all our results. The results of the two-wave approximation given by putting $M = -1$ and $\omega_{-1} = 1$ in Appendix II are as follows:

$$\eta_{-1}^t = \left(\frac{c}{\sqrt{p_0 p_{-1}}\,\gamma} \sin \gamma k_0 d \right)^2 \tag{32}$$

where

$$c = \delta n_e (s_{-1} \cos\theta - p_{-1} \sin\theta)/4$$
$$\Delta = (n_o^2 - p_{-1}^2 - s_{-1}^2)/4p_{-1}$$
$$\gamma = \sqrt{\frac{c^2}{p_0 p_{-1}} + \Delta^2}$$
$$p_0 = n_e \cos\theta_r \tag{33}$$

are also shown by the dashed curves. As seen in Fig. 4(b), TM_1 and TE_2 waves cannot be neglected due to the relatively large value of δ and small value of n_k although the Bragg condition is not satisfied exactly for $M = 1$.

Fig. 6 shows the variation of η_m^t with modulation index δ for fixed values of $\delta k_0 d = 2.0$ in Fig. 4(a), where $\bar{m}$ was retained up to $\bar{m} = 4$ for larger values of δ. It can be seen from Fig. 6 that η_{-1}^t begins to deviate from the two-wave approximation near $\delta > 0.01$ and that the deviation increases considerably for $\delta > 0.1$ with the appearance of the higher order diffractions, showing the limit of the two-wave approximation. In the practical applications, the quantity δ is usually of the order of 10^{-3} and then the two-wave approximation will give fairly exact results.

So far we put $\omega = 1$ because the values of $\omega_r = \Omega/\omega_0$ are the order of 10^{-6} in practice. However, the theoretical

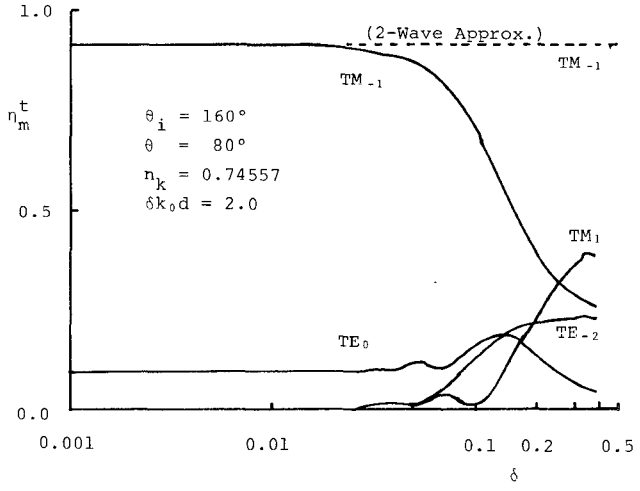

Fig. 6. Variation of the diffraction efficiencies with the modulation index.

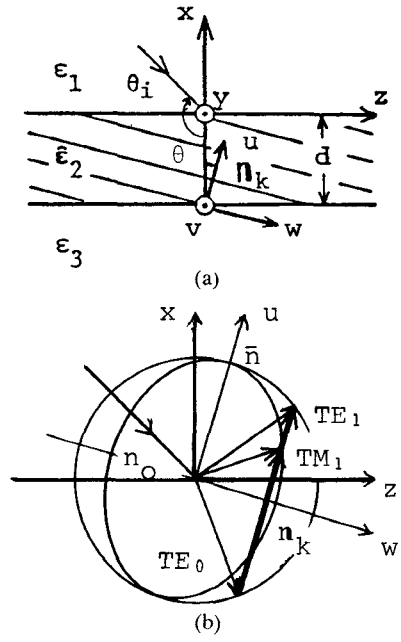

Fig. 7. Optical diffraction by a cholesteric liquid crystal. (a) Geometry. (b) Backward Bragg diffraction.

analysis still holds for $\omega \neq 1$. We then show some effects of time-varying medium in Fig. 4(c) by hypothetically putting $\omega_r = 0.03 \sim 0.05$. Other parameter values are the same as those in Fig. 4(a). The calculations were performed by retaining up to $\bar{m} = 7$ because the converence of the solution becomes poorer due to the parametric coupling in the time-varying medium. As can be seen from the figure, the diffraction efficiency of the TM_{-1} wave is decreased due to both the parametric coupling and the deviation from the true Bragg condition. This can also be anticipated from (A4) and (A7) in Appendix II.

B. Optical Diffraction by a Cholesteric Liquid Crystal (CLC)

As shown in Fig. 7, let the helical axis of a CLC with pitch P be along the u axis, which is inclined to the surface normal by an angle θ in the xz plane. The tensor permittivity of the CLC for the uvw coordinate system is given by

$$\hat{\epsilon}' = \bar{\epsilon}\begin{bmatrix} 1-\delta & 0 & 0 \\ 0 & 1-\delta\cos 2\alpha & \delta\sin 2\alpha \\ 0 & \delta\sin 2\alpha & 1+\delta\cos 2\alpha \end{bmatrix} \tag{34}$$

where

$$\begin{aligned} \bar{\epsilon} &= (\epsilon_w + \epsilon_u)/2 = \bar{n}^2 \\ \delta &= (\epsilon_w - \epsilon_u)/(\epsilon_w + \epsilon_u) \\ \epsilon_u &= \epsilon_v = n_o^2 \qquad \epsilon_w = n_e^2 \\ \alpha &= 2\pi u/P. \end{aligned} \tag{35}$$

This tensor permittivity can be represented by an ellipsoid in which the $\epsilon_u = \bar{\epsilon}(1-\delta)$ principal axis is always parallel to the u axis, and the two other principal axes $\epsilon_v = \bar{\epsilon}(1-\delta)$ and $\epsilon_w = \bar{\epsilon}(1+\delta)$ spiral around the u axis with pitch $P = 2u/\alpha$ [10], [11]. According to (34), the structure is periodic along the u axis with a space period $\Lambda = P/2$. Since the quantity δ expressing the periodic variation of the tensor permittivity in the CLC is usually of the order of 10^{-1}, the approximate analysis may not always give correct results and the 4×4 matrix method is used for precise calculations. However, the method cannot be applied to the case where the helical axis of the CLC is not perpendicular to the surface. Such situations may be realized through the orienting effect of boundaries [11].

The tensor permittivity for the xyz coordinate system is then obtained by rotating the old coordinate frame about the v axis through an angle θ and its elements become

$$\begin{aligned} \epsilon_{xx} &= \bar{\epsilon}(1-\delta\cos^2\theta + \delta\sin^2\theta\cos 2\alpha) \\ \epsilon_{yy} &= \bar{\epsilon}(1-\delta\cos 2\alpha) \\ \epsilon_{zz} &= \bar{\epsilon}(1-\delta\sin^2\theta + \delta\cos^2\theta\cos 2\alpha) \\ \epsilon_{xy} &= \epsilon_{yx} = -\bar{\epsilon}\delta\sin\theta\sin 2\alpha \\ \epsilon_{yz} &= \epsilon_{zy} = \bar{\epsilon}\delta\cos\theta\sin 2\alpha \\ \epsilon_{xz} &= \epsilon_{zx} = -\bar{\epsilon}\delta\cos\theta\sin\theta(1+\cos 2\alpha) \end{aligned} \tag{36}$$

where

$$\boldsymbol{n}_k \cdot \boldsymbol{r} = 2\alpha \qquad n_k = \lambda/\Lambda = 2\lambda/P \tag{37}$$

and in matrix form, for instance,

$$\epsilon_{yy} = \frac{\bar{\epsilon}}{2}\begin{bmatrix} & & \vdots & & \\ & 2 & -\delta & 0 & 0 & \\ & -\delta & 2 & -\delta & 0 & \\ \cdots & & & & & \cdots \\ & 0 & -\delta & 2 & -\delta & \\ & 0 & 0 & -\delta & 2 & \\ & & \vdots & & & \end{bmatrix},$$

$$\epsilon_{yz} = \frac{j\bar{\epsilon}\delta\cos\theta}{2}\begin{bmatrix} & & \vdots & & \\ & 0 & -1 & 0 & 0 & \\ & 1 & 0 & -1 & 0 & \\ \cdots & & & & & \cdots \\ & 0 & 1 & 0 & -1 & \\ & 0 & 0 & 1 & 0 & \\ & & \vdots & & & \end{bmatrix}, \text{ etc.} \tag{38}$$

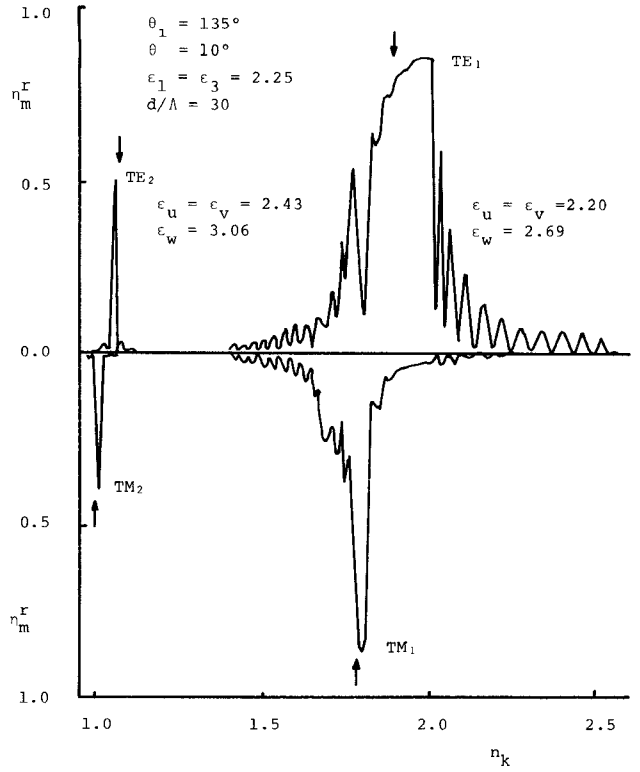

Fig. 8. The diffraction efficiencies of reflected waves (reflection spectra) for the incidence of a TE wave.

Fig. 8 shows the diffraction efficiencies of the reflected waves (reflection spectra) η_m^r near the first- and second-order Bragg conditions, where $\theta_i = 135°$, $\theta = 10°$, and $d/\Lambda = 30$. The parameter values of the CLC are chosen as $n_e^2 = 2.690$, $n_o^2 = 2.200$, and $\delta = 0.1002$ for $M = 1$, and $n_e^2 = 3.060$, $n_o^2 = 2.430$, and $\delta = 0.11475$ for $M = 2$, respectively, and those of the uniform regions are chosen as $\epsilon_1 = \epsilon_3 = 2.25$ [14].

The calculations were performed by retaining up to $\bar{m} = 3$ with energy conservation error of 10^{-8} as before. Since all diagonal and nondiagonal elements ϵ_{ij} have periodic variations, both TE–TE and TE–TM diffractions take place simultaneously. The arrows in the figure at $n_k = 1.780$, $n_k = 1.895$ and $n_k = 1.007$, $n_k = 1.069$ show the first- and second-order Bragg reflection points corresponding to TE–TM and TE–TE diffractions. In this backward diffraction, some of the lower order eigenvalues κ_m have complex values near this Bragg points that correspond to the first- and second-order stopbands. Outside these stopbands, these eigenvalues have real values that correspond to the passband in which selective reflections do not occur. As can be seen from Fig. 8, the first-order reflection spectra oscillate rapidly with the variation of n_k due to the effect of both multimode coupling and multiple reflections at the boundaries, and they cannot be expressed exactly by the approximate two-wave analysis. Fig. 9 shows the variation of η_m^r and η_m^t with the thickness of the CLC at $n_k = 1.790$ in Fig. 8. The small beats due to the multiple reflection disappear gradually with increasing d/Λ because the incident TE_0 wave is totally converted to reflected TE_1 and TM_1 waves before it reaches the other boundary for larger values of d/Λ.

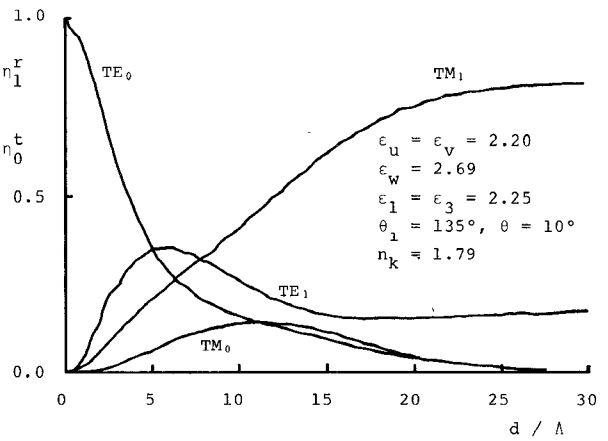

Fig. 9. Variation of the diffraction efficiencies with the thickness of the CLC.

TABLE I
ACCURACY OF THE FIRST-ORDER REFLECTED DIFFRACTION EFFICIENCIES WITH δ AS A PARAMETER FOR THE INCIDENCE OF TE WAVES

δ		0.05	0.1	0.2	0.3
		TE_0 - TE_1 η_1^r			
$\bar{m}$	$2\bar{m}+1$				
1	3	0.053897	0.161734	0.729490	0.835059
2	5	0.054371	0.176875	0.733845	0.828723
3	7	0.054371	0.176876	0.733863	0.828928
4	9	0.054371	0.176876	0.733863	0.828929
5	11	0.054371	0.176876	0.733863	0.828929
6	13	0.054371	0.176876	0.733863	0.828929
		TE_0 - TM_1 η_1^r			
$\bar{m}$	$2\bar{m}+1$				
1	3	0.157467	0.824571	0.045721	0.019838
2	5	0.157633	0.810122	0.036696	0.024229
3	7	0.157633	0.810122	0.036701	0.024267
4	9	0.157633	0.810122	0.036701	0.024267
5	11	0.157633	0.810122	0.036701	0.024267
6	13	0.157633	0.810121	0.036701	0.024267

$\theta_i = 135°$, $\theta = 10°$, $d/\Lambda = 30$, $n_k = 1.79$.

C. Accuracy of the Numerical Calculations

Table I shows the accuracy of the solution by the truncation of the matrix $\boldsymbol{C}$ in the case of Fig. 8 with the fixed value of d/Λ and $\bar{\epsilon}$ with δ as a parameter, where $\bar{m}$ is the order of space harmonics and $2\bar{m}+1$ is the total number of space harmonics used in the calculations. In this case, $\epsilon_u = \epsilon_v = \bar{\epsilon}(1-\delta)$, and $\epsilon_w = \bar{\epsilon}(1+\delta)$ varies with δ so that the Bragg condition is satisfied only for $\delta = 0.1$. From this table, it can be seen that the solutions have almost converged at $\bar{m} = 3$. Since the other examples showed similar results, most of the calculations were performed by retaining up to $\bar{m} = 3$–4 with the error in the power-conservation relation of the order of 10^{-8} in all our results.

IV. Conclusions

A rigorous analysis of wave diffraction by space–time periodic anisotropic media has been formulated. The direction of the grating vector, the modulation of the medium,

and the polarization of the incident plane wave are all arbitrary. The solution is reduced to an eigenvalue problem of the coupling matrix whose elements are given by a unified form so that calculations can be performed by systematic matrix calculations. The method applies to arbitrarily thick or lossy media without encountering overflow problems in the computations by giving boundary condition in somewhat modified form. As numerical examples, optical diffraction by an acoustic wave and by a CLC are considered, and the results are compared with the approximate two-wave analysis. Any level of accuracy can be obtained by increasing the space–time harmonics. Although the retention of relatively few harmonics is sufficient for continuously modulated time-invariant media, usually more harmonics are necessary for time-varying media because the effect of parametric coupling increases with an increase in modulating frequency.

Appendix I
Derivation of the Coupling Matrices

By substituting (6) into (3), multiplying $\exp\{j(\boldsymbol{n}_m \cdot \boldsymbol{r} - \omega_m t)\}$ on both sides, and integrating over y, z, t for each period, we get the infinite set of coupled-wave equations

$$\begin{aligned}
&\frac{\partial e_{ym}}{\partial x} - jp_m e_{ym} + jq_m e_{xm} = -j\omega_m h_{zm} \\
&\frac{\partial e_{zm}}{\partial x} - jp_m e_{zm} + js_m e_{xm} = j\omega_m h_{ym} \\
&\frac{\partial h_{ym}}{\partial x} - jp_m h_{ym} + jq_m h_{xm} = j\omega_m \sum_l \sum_\iota \epsilon_{zl,l-m} e_{il} \\
&\frac{\partial h_{zm}}{\partial x} - jp_m h_{zm} + js_m h_{xm} = -j\omega_m \sum_l \sum_\iota \epsilon_{yl,l-m} e_{il} \qquad \text{(A1)}
\end{aligned}$$

$$\begin{aligned}
q_m e_{zm} - s_m e_{ym} &= \omega_m h_{xm} \\
-q_m h_{zm} + s_m h_{ym} &= \omega_m \sum_l \sum_\iota \epsilon_{xl,l-m} e_{il}. \qquad \text{(A2)}
\end{aligned}$$

Equations (A2) can be solved for e_{xm} and h_{xm}. Then, substituting these into (A1), we get the coupled-wave equations (10) in matrix form with $\boldsymbol{C}$ and $\boldsymbol{D}$ given by (12)–(14).

Appendix II
Derivation of Approximate Two-Wave Analysis

If we retain only $m = 0$ and $m = M$ terms in the rigorous equation (10) with $\hat{\epsilon}$ given by (29) and eliminate $h_{im}(i = y, z)$, we get the coupled differential equations for e_{im} with the second derivatives. Neglecting further the terms of $d^2 e_{im}/dx^2$, $\delta de_{im}/dx$, and $\delta^2 e_{im}$ for small values of δ, we get the following differential equations:

$$\begin{aligned}
\frac{de_{y0}}{dx} &= j\frac{cn_o}{p_0 p_M} e_{zM} \\
\frac{de_{zM}}{dx} + 2j\Delta e_{zM} &= j\frac{c}{n_o} e_{y0} \qquad \text{(A3)}
\end{aligned}$$

with

$$\begin{aligned}
c &= \delta n_e (s_M \cos\theta - p_M \sin\theta)/4 \\
\Delta &= (\omega_M^2 n_o^2 - p_M^2 - s_M^2)/4p_M \qquad \text{(A4)}
\end{aligned}$$

where c and Δ represent the effective coupling coefficient and the deviation from the Bragg condition, respectively. The solution of (A3) under the boundary conditions of $e_{y0}(0) = 1$ and $e_{zM}(0) = 0$ becomes

$$\begin{aligned}
e_{y0} &= \left(\cos\gamma x + j\frac{\Delta}{\gamma}\sin\gamma x\right)\exp(-j\Delta x) \\
e_{zM} &= j\frac{c}{n_o\gamma}\sin\gamma x \exp(-j\Delta x) \qquad \text{(A5)}
\end{aligned}$$

with

$$\gamma = \sqrt{\frac{c^2}{p_0 p_M} + \Delta^2}. \qquad \text{(A6)}$$

The zeroth- and Mth-order powers along the x direction are ${}^{E}P_0 = p_0|e_{y0}|^2$ and ${}^{M}P_M = \omega_M |n_o e_{zM}|^2/p_M$. Since x represents the normalized variable, the diffraction efficiency becomes

$$\eta_M^t = \frac{{}^{M}P_M(-k_0 d)}{{}^{E}P_0(0)} = \omega_M \left(\frac{c}{\sqrt{p_0 p_M}\,\gamma}\sin\gamma k_0 d\right)^2. \qquad \text{(A7)}$$

Equation (A7) shows that the diffraction efficiency is increased or decreased by a factor ω_M due to the parametric coupling in the time-varying medium.

Acknowledgment

The authors wish to express their thanks to M. Kominami for his valuable discussions. Thanks are also due to H. Teraguchi for his assistance in the numerical calculations.

References

[1] H. Kogelnik, "Coupled wave theory for thick hologram gratings," *Bell Syst. Tech. J.*, vol. 48, pp. 2909–2947, Nov. 1969.
[2] R S. Chu and T. Tamir, "Guided-wave theory of light diffraction by acoustic microwaves," *IEEE Trans. Microwave Theory Tech.*, vol. MTT-18, pp. 486–504, Aug. 1970.
[3] R. S. Chu and T. Tamir, "Wave propagation and dispersion in space–time periodic media," *Proc. Inst. Elec. Eng.*, vol. 119, pp. 797–806, July 1972.
[4] S. T. Peng, T. Tamir, and H. L. Bertoni, "Theory of periodic dielectric waveguides," *IEEE Trans. Microwave Theory Tech.*, vol. MTT-23, pp. 123–133, Jan. 1975.
[5] R. S. Chu and J. A. Kong, "Modal theory of spatially periodic media," *IEEE Trans. Microwave Theory Tech.*, vol. MTT-25, pp. 18–24, Jan. 1977.
[6] M. G. Moharam and T. K. Gaylord, "Rigorous coupled-wave analysis of planar-grating diffraction," *J. Opt. Soc. Amer.*, vol. 71, pp. 811–818, July 1981.
[7] T. K Gaylord and M. G. Moharam, "Analysis and application of optical diffraction by gratings," *Proc. IEEE*, vol 73, pp. 894–937, May 1985.
[8] R. W. Dixon, "Acoustic diffraction of light in anisotropic media," *IEEE J. Quantum Electron* , vol. QE-3, pp 85–93, Feb. 1967.
[9] L L. Hope, "Brillouin scattering in birefringent media," *Phys. Rev.*, vol 166, pp. 883–892, Feb. 1968.
[10] D. W Berreman, "Optics in stratified and anisotropic media: 4×4-matrix formulation," *J. Opt. Soc. Amer.*, vol. 62, pp. 502–510, Apr. 1972.

[11] V. A. Belyakov, V. E. Dmitrienko, and V. P. Orlov, "Optics of cholesteric liquid crystals," *Sov. Phys.—Usp.*, vol. 22, pp. 63–88, Feb. 1979.
[12] S. Garoff, R. B. Meyer, and R. Barakat, "Kinematic and dynamic light scattering from the periodic structure of a chiral smectic C liquid crystal," *J. Opt. Soc. Amer.*, vol. 68, pp. 1217–1225, Sept. 1978.
[13] M. A. Peterson, "Light propagation and light scattering in cholesteric liquid crystals," *Phys. Rev.*, vol. A 27, pp. 520–527, Jan. 1983.
[14] C. Oldano, E. Miraldi, and P. Taverna Valabrega, "Dispersion relation for propagation of light in cholesteric liquid crystals," *Phys. Rev.*, vol. A 27, pp. 3291–3299, June 1983.
[15] H. L. Ong and R. B. Meyer, "Geometrical-optics approximation for the electromagnetic fields in layered-inhomogeneous liquid-crystalline structures," *J. Opt. Soc. Amer.*, vol. A 2, pp. 198–201 Feb. 1985.
[16] P. Yeh, "Electromagnetic propagation in birefringent layered media," *J. Opt. Soc. Amer.*, vol. 69, pp. 742–756, May 1979.
[17] K. Rokushima and J. Yamakita, "Analysis of anisotropic dielectric gratings," *J. Opt. Soc. Amer.*, vol. 73, pp. 901–908, July 1983.
[18] R. F. Adrion, "The so-called Doppler shift in Bragg cells," *Proc. IEEE*, vol. 58, pp. 1391–1393, Sept. 1970.
[19] J. Askne, "Bragg's law generalized to time–space periodic media," *Proc. IEEE*, vol. 59, p. 1350, Sept. 1971.

✠

Katsu Rokushima (M'64) received the B.S. and Ph.D degrees in electrical engineering from Osaka University, Osaka, Japan, in 1950 and 1971, respectively.

He joined the University of Osaka Prefecture, Sakai, in 1950, where he did research in microwave engineering. Since 1973, he has been a Professor of Electrical Engineering at the University of Osaka Prefecture. His research interests include electromagnetic field problems as they relate to microwave and millimeter-wave circuits, antennas, optical waveguides, and diffraction gratings.

Dr. Rokushima is a member of the Optical Society of America, the IEE of Japan, the IECE of Japan, and the Institute of TV Engineers of Japan.

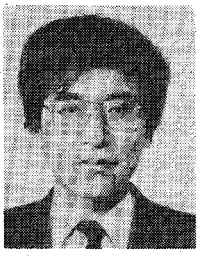

Jiro Yamakita received the B.S. and M.S. degrees in electrical engineering from Kyoto Technical University in 1969 and 1971, respectively, and the Ph.D. degree in electrical engineering from the University of Osaka Prefecture in 1981.

He was with the Mitsubishi Electric Co. Ltd., Tokyo, from 1971 to 1973. He is presently a Research Associate at the University of Osaka Prefecture engaged in research on integrated optics for optical communications, in particular periodic and random dielectric optical waveguides.

Dr. Yamakita is a member of the IECE of Japan.

✠

Shizuo Mori received the B.S. and M.S. degrees in electrical engineering from the University of Osaka Prefecture in 1959 and 1961, respectively.

He joined the University of Osaka Prefecture in 1961, where he has done research on microwave circuits and has been an Assistant Professor since 1973. His research interests include dielectric waveguides and planar and finline circuits in the microwave and millimeter-wave regions.

Mr. Mori is a member of the IECE of Japan.

✠

Kenji Tominaga received the B.S. and M.S. degrees in electrical engineering from the University of Osaka Prefecture in 1984 and 1986, respectively. He joined the Mitsubishi Electric Co. Ltd., Tokyo, in 1986.